Guo, Yingying; Dai, Xiangdong; Kittisak Jermsittiparsert; Razmjooy, Navid

Article

An optimal configuration for a battery and PEM fuel cell-based hybrid energy system using developed Krill herd optimization algorithm for locomotive application

Energy Reports

Provided in Cooperation with:
Elsevier

Suggested Citation: Guo, Yingying; Dai, Xiangdong; Kittisak Jermsittiparsert; Razmjooy, Navid (2020) : An optimal configuration for a battery and PEM fuel cell-based hybrid energy system using developed Krill herd optimization algorithm for locomotive application, Energy Reports, ISSN 2352-4847, Elsevier, Amsterdam, Vol. 6, pp. 885-894, https://doi.org/10.1016/j.egyr.2020.04.012

This Version is available at:
https://hdl.handle.net/10419/244086

Energy Reports 6 (2020) 885–894

Contents lists available at ScienceDirect

Energy Reports

journal homepage: www.elsevier.com/locate/egyr

Research paper

An optimal configuration for a battery and PEM fuel cell-based hybrid energy system using developed Krill herd optimization algorithm for locomotive application

Yingying Guo [a,b], Xiangdong Dai [a], Kittisak Jermsittiparsert [c,*], Navid Razmjooy [d]

[a] School of Materials Science and Engineering, Central South University of Forestry and Technology, Changsha 410004, China
[b] School of Architecture and Civil Engineering, Huanghuai University, Zhumadian 463000, China
[c] Social Research Institute, Chulalongkorn University, Bangkok 10330, Thailand
[d] Department of Engineering, Tafresh University, Tafresh, Iran

ARTICLE INFO

Article history:
Received 1 January 2020
Received in revised form 13 March 2020
Accepted 4 April 2020
Available online xxxx

Keywords:
Hybrid energy system
Lithium-ion battery
Energy management optimization
Locomotive
Converged Krill herd optimization algorithm
PEM fuel cell

ABSTRACT

A new methodology has been proposed for optimal size selection of a hybrid energy system (HES) including lithium-ion battery and polymer electrolyte membrane (PEM) fuel cell to supply the driving force of a locomotive. The main purpose is to minimize the total cost of HES with different constraints including the capacity constraint of the battery and the fuel cell state-of-charge limit The optimization problem has been solved based on a new improved model of the Krill Herd (KH) algorithm, converged krill herd optimization algorithm (CKH). Simulation results are analyzed based on the average power demand, speed demand of the locomotive, and the locomotive slope. The results of the presented CKH algorithm have been compared with the standard KH and PSO algorithm and the results declared that the total cost for HES based on CKH has the minimum value such that the value for the CKH for 0%, 1%, and 2% slope are 3.15×10^6, 3.56×10^6, and 3.93×10^6 toward KH with 3.47×10^6, 4.01×10^6, and 4.56×10^6 and PSO with 3.74×10^6, 4.27×10^6, and 4.72×10^6 HES, respectively.

1. Introduction

The development of vehicles based on internal combustion engines, especially automobiles, is one of the great achievements of human science and technology (Ghadimi, 2015; Haixiong et al., 2020; Firouz and Ghadimi, 2015). This has led to serious problems for the environment and human life (Hosseini et al., 2012, 2011). Air pollution, global warming and limited fossil fuel resources are the major problems (Hosseini et al., 2013). In recent decades, extensive research has been done on clean and efficient fuel-efficient vehicles, including electric vehicles, electric hybrids, and fuel cells. These vehicles can be a good alternative to today's vehicles in the future (Dongmin et al., 2019; Shamel and Ghadimi, 2016; Dongmin et al., 2020; Seyed-Shenava and Khezri, 2014).

A fuel cell (FC) stack is an energy converter to convert the fuel and oxidizer energy directly into electrical energy. High efficiency, low operating temperature (used as a driving force) and lack of pollutions such as sulfur (SO_x) and nitrogen oxides (NO_x), low vibration and noise, low efficiency depending on the size of the system, and a variety of fuel sources (renewable and non-renewable) are some of characteristics that turn Fuel cell as one of the popular options for replacing internal combustion engines and consequently a viable solution to reduce energy and environmental problems caused by direct fossil fuel consumption in the future (Aghajani and Ghadimi, 2018; Liu et al., 2017). Currently, this energy converter is widely studied around the world in order to be competitive with combustion engines in various aspects, including price, fuel supply, stability, and safety. One of the problems of the fuel cell-based system is that due to their new technology, the cost of preparing them is a little high. Therefore, this paper focus on resolving the mentioned problems. The main innovation of the present work is highlighted below:

1. Optimal configuration of a Hybrid Energy System for Locomotive Applications.
2. Using an optimal configuration for Battery and PEM fuel cells in the Hybrid Energy System.
3. Optimal Size selection of the Battery and PEM fuel cell in the Hybrid Energy System.
4. Using Chinese locomotive class HXD_3G as a practical case study.
5. Proposing a new version of the Krill Herd optimization algorithm for optimization of the sizes of the HES components.

* Corresponding author.
E-mail address: kittisak.j@chula.ac.th (K. Jermsittiparsert).

https://doi.org/10.1016/j.egyr.2020.04.012

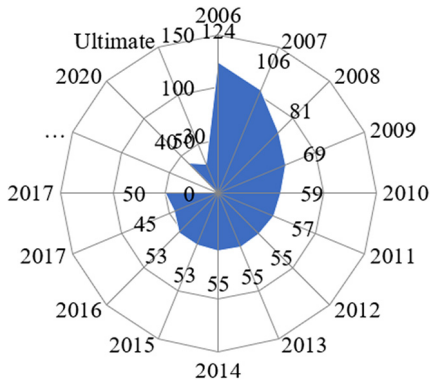

Fig. 1. Model cost of FC system ($\$/kW_{net}$) over the time (year).

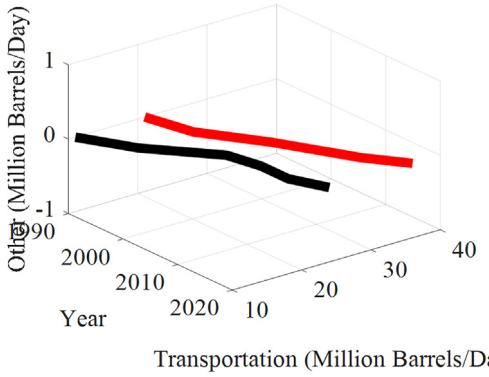

Fig. 2. Fuel consumption chart for transportation and other sectors (Mirzapour et al., 2019).

2. Literature review

In recent years, research funded by DOE Hydrogen and Fuel Cell organization claimed that they succeed to reduce the cost of transportation fuel cells by 60% since 2006. They also proofed that Fuel cell reliability has improved by a factor of 4 since 2006 (Gollou and Ghadimi, 2017) (see Fig. 1).

Fuel cells do not also produce negligible pollutants such as SO_x and NO_x, particulate matter and organic compounds, but also produce significantly less CO and CO_2 pollutants than combustion engines (CO and CO_2 production in the fuel cell are 0.25% and 46% of the combustion engine).

The transportation industry, followed by automobiles, is a major contributor to fossil fuel consumption; Fig. 2 shows the fuel consumption chart for transportation and other sectors (Mirzapour et al., 2019). As shown in Figure, on average, 49% of the world's fuel is spent on industrial and developing countries for transportation. It is projected that fuel consumption in the transport sector is projected to increase by about 11.4 million barrels per day from the year 1997 to the year 2020 in industrialized countries. The same trend is also seen in developing countries, with almost 50% devoted to this sector in the year. On this basis, there is high interesting today in the automobile industry for the use of more efficient vehicles than the internal combustion engines and the use of clean fuels.

Recently, several research works have been developed about the hybrid energy system (HES) based on PEMFC-battery in transportation applications. The literature has been principally divided into two research directions. The first direction is to use different control techniques for handling the energy management strategy (EMS) and the second direction is the works that have been focused on the optimization techniques. The optimization techniques have usually two types including energy management optimization (EMO) method to optimize EMS and design optimization (DO) method for optimizing the HES component sizing. The method of optimization can be done by classical methods and like dynamic programming (Firouz et al., 2016), non-linear programming (Hamian et al., 2018), and meta-heuristics like genetic algorithm and particle swarm optimization (Leng et al., 2018). Different works have been worked about the application of energy management strategy on electric vehicles (Akbary et al., 2019). For example, Ahmadi et al. (Homayoun et al., 2018) developed a hybrid FC-based electric vehicle with ultra-capacitor (FCHEV) and battery in terms of performance and fuel economy based on optimized EMS. An optimized fuzzy-based strategy was presented for controlling the FCHEV system. Final results were assessed for showing the system efficiency and showed less than 2% for the battery charge level variations.

Zhou et al. (Khodaei et al., 2018) proposed an online EMS based on a fractional-order extremum seeking (ES) approach. The presented technique was an improved version of the traditional integer-order ES method along with fractional-order Oustaloup approximation evaluation to improve the speed of method convergence with higher reliability. For analyzing the system's reliability and speed, an experimental test was done. The final results declared that using the proposed technique for controlling the PEMFC based system is completely efficient (Eslami et al., 2019; Gao et al., 2019; Saeedi et al., 2019).

Hong et al. (2018) introduced a dynamic power factor-based EMS for a locomotive using hybrid fuel cell and battery. The method had a self-adaption function for obtaining less H_2 consumption and higher performance in different driving cycles. The efficiency of the system was finally analyzed to determine each part's capability.

Bendjedia et al. (2018) presented an optimized sizing technique for an ESS including a lithium-ion battery and a fuel cell for providing the power to a lightweight vehicle for 700 km. At last, for showing the effect of the ESS design driving cycles, it was analyzed based on New European Driving Cycle)NEDC(and then the system durability was assessed. The main purpose of the present work is to use HES based on PEM fuel cells in transportation. From the literature, it can be observed that there are a few types of research about the application of the PEM fuel cell in locomotives. The literature review shows that there is no (or maybe little) research about mathematical modeling of EMO and DO for the PEMFC-battery HES in the locomotive application. This reason has been a big motivation to work on it. Generally, the primary objective of the presented study is to improve a hybrid battery-PEM fuel cell HES model for supplying the tractive effort of a locomotive. For improving the system efficiency, the sizes of the HES components have been obtained by a new improved version of the krill herd optimization algorithm. The aim of the optimization here is to minimize the overall cost of the HES components by considering different constraints such as instantaneous power demand, battery SOC, and PEMFC capacity. The final results have been compared with some different methods from the literature. In the following, Section 2 describes the mathematical model of the system. Section 3 declares the methodology for EMS. Section 4 introduced a detailed explanation for the optimization of the studied HES. Section 5 determines the method of solving the problem. Simulation results are illustrated in Section 4 and the work has been concluded in Section 5.

3. Mathematical model of the system

The modeled HES system contains PEM fuel cell and a pack of lithium-ion batteries as the main energy source and the backup

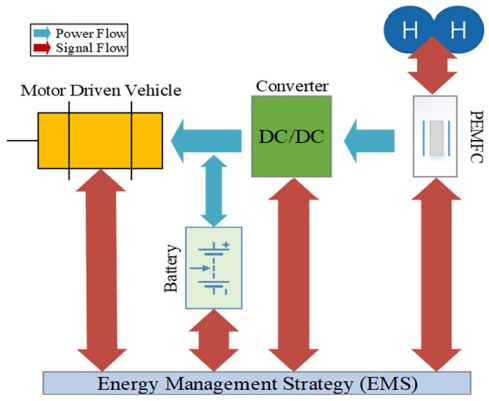

Fig. 3. Diagram of the hybrid PEMFC/battery system.

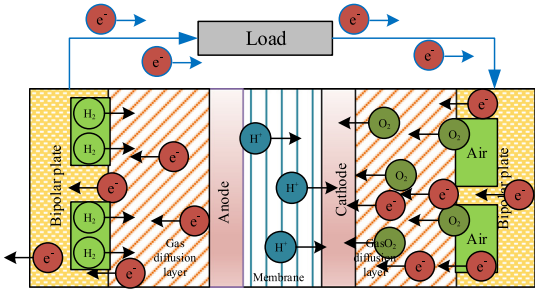

Fig. 4. A general schematic of the PEMFC stack.

energy source, respectively thanks to its several benefits such as high energy and power density and longer lifetime. Here, a 100 Wh/kg lithium manganese oxide (Li_2MnO_2The) battery is utilized for simulation (Geng et al., 2014). Fig. 3 shows the diagram of the Hybrid PEMFC/battery system based on HES. Indeed, the HES system is introduced to replace the diesel engine of the Chinese locomotive class HXD_3G that is utilized in china railways since 2015.

Due to several numbers of intermediate stops in the intercity passenger trains between the terminal stations, the speed of the trains has been changed continuously which provides floating power demand for the train. The minimum size of the PEMFC has been selected to be higher than the power demand of the locomotive due to the PEM fuel cell slow dynamic response. The battery stack is utilized for absorbing the generated power during the regenerative braking. In the following, the mathematical model of the hybrid locomotive parts has been given.

3.1. The model of PEMFC stack

Fuel cell stacks are some kinds of energy resources that convert chemical energy directly into electricity with no combustion. Thanks to their clean energy production and high efficiency, Fuel cells have been turned into one of the most popular energy conversion systems (Luo et al., 2015; Razmjooy et al., 2018). One of the most used fuel cells is the proton-exchange membrane fuel cells (PEM fuel cell). A PEM fuel cell includes three principal parts: an anode, a cathode, and an electrolyte membrane. Fig. 4 shows the general schematic of a PEMFC stack.

In a PEM fuel cell, H_2 has been ionized by anode to generate protons and electrons. Afterward, the electrons have been transmitted into an external circuit for the current generation and H_2 protons transmitted into the membrane by remising molecules to each other. In the cathode side, O_2 has been synthesized by the protons from the anode and the electrons from the external circuit by generating water and heat. The total output voltage of a PEMFC has been illustrated in the following (Corrêa et al., 2004; Aouali et al., 2017):

$$V_o = N_{\mathrm{nc}} \times \left(E_N - E_{\mathrm{op}} - E_O - E_{\mathrm{ops}}\right) \tag{1}$$

where, N_{nc} defines the number of connected cells, E_{op} describes the activation over-potential of the cells, E_O represents the Ohmic voltage drop of the cells, E_{ops} determines the over-potential saturation in the cells, and E_N is the Nernst equation which declares the cell reversible voltage per cell and is achieved as follows (Kandidayeni et al., 2019):

$$E_N = 1.23 - 8.5 \times 10^{-4} \times (T_{\mathrm{FC}} - 298.15) + 4.31 \times 10^{-5} \times T_{\mathrm{FC}} \times \left[ln\left(P_{H_2}\right) + 0.5 \times ln\left(P_{O_2}\right)\right] \tag{2}$$

here,

$$P_{\mathrm{H_2}} = \frac{R_{\mathrm{ha}} \times P_{\mathrm{H_2O}}}{2} \left[\frac{1}{\frac{R_{\mathrm{ha}} \times P_{\mathrm{H_2O}}}{P_a} \times e^{\frac{1.635 I_{\mathrm{FC}}/A}{T^{1.334} I_{\mathrm{FC}}}}} - 1 \right] \tag{3}$$

$$P_{\mathrm{O_2}} = R_{\mathrm{hc}} \times P_{\mathrm{H_2O}} \left[\frac{1}{\frac{R_{\mathrm{hc}} \times P_{\mathrm{H_2O}}}{P_c} \times e^{\frac{1.635 I_{\mathrm{FC}}/A}{T^{1.334} I_{\mathrm{FC}}}}} - 1 \right] \tag{4}$$

here, A represents the membrane active area, I_{FC} describes the fuel cell operating current, R_{hc} and R_{ha} determine the vapor relative humidity in electrodes, P_a and P_c describe the anode and the cathode inlet partial pressures, respectively.

For the PEMFC operating temperature, the saturation vapor pressure is formulated as follows:

$$\log 10\left(P_{\mathrm{H_2O}}\right) = 0.0295 \times (T_{\mathrm{FC}} - 273.15) - 9.18 \times 10^{-5} T_c^2 + 1.4 \times 10^{-7} T_c^3 - 2.18 \tag{5}$$

The value for the reference temperature is considered 25 °C.

The Ohmic voltage drop for all the cells is modeled by the following equivalent:

$$E_O = I_{\mathrm{FC}} \times (R_m + R_c) \tag{6}$$

here,

$$R_m = \rho_m \times l \times S^{-1} \tag{7}$$

$$\rho_m = \frac{181.6 \times \left[0.062 \times \left(\frac{T_{\mathrm{FC}}}{303}\right)^2 \times \left(\frac{I_{\mathrm{FC}}}{S}\right)^{2.5} + 0.03\left(\frac{I_{\mathrm{FC}}}{S}\right) + 1\right]}{\left[\lambda - 0.063 - 3\left(\frac{I_{\mathrm{FC}}}{S}\right)\right] \times e^{\frac{T_{\mathrm{FC}} - 303}{T_{\mathrm{FC}}}}} \tag{8}$$

The over-potential activation loss is formulated as follows:

$$E_{\mathrm{op}} = -\left[\gamma_1 + \gamma_2 T_{\mathrm{FC}} + \gamma_3 T_{\mathrm{FC}} \ln\left(C_{\mathrm{O_2}}\right) + \gamma_4 T_{\mathrm{FC}} \ln\left(I_{\mathrm{FC}}\right)\right] \tag{9}$$

here, $C_{\mathrm{O_2}}$ represents the saturation value of the O_2 in the catalytic interface of the cathode (mol/cm^3) and are achieved as follows:

$$C_{\mathrm{O_2}} = \frac{P_{\mathrm{O_2}}}{5.1 \times 10^6} \times e^{\frac{498}{T_{\mathrm{FC}}}} \tag{10}$$

and,

$$\gamma_2 = 29 \times 10^{-4} + 21 \times 10^{-5} \ln(A) + 43 \times 10^{-6} \ln(C_{\mathrm{H_2}}) \tag{11}$$

here, $C_{\mathrm{H_2}}$ represents the saturation value of the H_2 in the catalytic interface of the cathode (mol/cm^3) and are achieved as follows:

$$C_{\mathrm{H_2}} = \frac{P_{\mathrm{H_2}}}{1.1 \times 10^6} \times e^{\frac{-77}{T_{\mathrm{FC}}}} \tag{12}$$

Table 1
The optimal parameter estimation extracted from Aghajani and Ghadimi (2018).

Parameter	Value	Parameter	Value
β_1	−1.03	$\beta_4 \times 10^{-5}$	−9.48
$\beta_2 \times 10^{-3}$	3.48	β	0.01
$\beta_3 \times 10^{-5}$	7.79	$R_c \times 10^{-4}$	1.63

And the over-potential saturation (E_{ops}) in each cell is as follows:

$$E_{\text{ops}} = -\beta \times ln\left(\frac{J_{max}^2 - J \times J_{max}}{J_{max}}\right) \tag{13}$$

here, S describes the membrane surface (cm^2), I_{FC} represents the fuel cell operating current, I describes the thickness of the membrane, β_i describes the empirical coefficients, T_{FC} determines the operating cell temperature (°), λ represents a controllable parameter, β determines a parametric coefficient, P_{H}, P_{O_2}, and $P_{\text{H}_2\text{O}}$ represents the partial pressure of the H_2, O_2, and H_2O, respectively, J and J_{max} are the standards and the maximum current densities, respectively, R_{ha} and R_{hc} represent the vapor relative humidity at anode and cathode, respectively, P_c and P_a describe the inlet pressure for the cathode and the anode, C_{H_2} and C_{O_2} are the hydrogen and oxygen (mol/cm^3) saturation, R_c and R_m describe the connections resistance and the membrane resistance. In this paper, for the unknown parameters, the optimum values from Aghajani and Ghadimi (2018) have been extracted which is illustrated in Table 1.

In the following, the efficiency of a PEMFC system is formulated as follows:

$$\eta_{\text{FC}} = \eta_{\text{fc}}\left(1 - \frac{P_{\text{fc}}^{\text{aux}}}{P_{\text{fc}}}\right) \tag{14}$$

here,

$$\eta_{\text{fc}} = \frac{P_{\text{fc}}}{P_{H_2}} \tag{15}$$

$$P_{\text{fc}} = V_o \times I_o \tag{16}$$

here, I_o describes the fuel cell stack current.

The total fuel consumption of the PEM fuel cell (mH_2) is formulated as follows:

$$C_{\text{FC}} = \int \frac{P_{\text{FC}}}{LHV \times \eta_{\text{FC}}(PLR)} dt \tag{17}$$

here, LHV describes the hydrogen lower heating value and $\eta_{\text{FC}}(PLR)$ is the PEM fuel cell efficiency map as a function of the part-load ratio (PLR) (Maleki and Rosen, 2017).

The corresponding heat generated, Q_{heat}, during the driving period is as follows:

$$Q_{heat} = C_{\text{FC}} \times LHV \tag{18}$$

Although, it should be considered that the existence of the auxiliary elements in the fuel cell system makes a restriction on the fuel cell net power output ratio which is because of the slow dynamic response of the auxiliary elements. In the present study, the limitation value, A is achieved as follows:

$$A = \frac{0.9\ of\ P_{\text{FC}}^{rated}}{T} \tag{19}$$

here, $T = 30$ s.

Finally,

$$P_{\text{FC}}(t) = A \times t + P_{\text{FC}}^0 \tag{20}$$

here, P_{FC}^0 describes the beginning of the deceleration/acceleration period.

3.2. Lithium-ion battery

The lithium-ion battery is a family of high-density rechargeable batteries. Unlike the disposable lithium battery, the lithium-ion battery uses a lithium-ion compound instead of metal lithium as the electrode (Bagal et al., 2018). Usually, lithium-ion batteries are considerably lighter than other kinds of rechargeable batteries of the same size. Lithium-ion batteries have been widely utilized in portable electronics. The utilized lithium-ion battery here is employed in the presented HES for assisting the output power of the PEMFC in the transient conditions. The instantaneous output power of the lithium-ion battery is achieved as follows:

$$P_b(t) = P_{Lo}(t) - P_{\text{FC}}(t) \tag{21}$$

where, $P_{Lo}(t)$ describes the total instantaneous power demand for the locomotive.

The positive value for $P_b(t)$ shows the discharging state, the negative value for the $P_b(t)$ implies to charging state of the operation and the zero value implies that the battery remains idle.

The SOC of the battery at any moment belongs to the SOC of the battery at the prior moment ($t - \Delta t$) and is obtained as follows:

$$SOC(t) = SOC(t - \Delta t) - \eta_b \times \frac{P_b(t)}{Q_{bc}} \Delta t \tag{22}$$

here, η_b represents the charging/discharging efficiency of the battery and is achieved by the following equation:

$$\eta_b = \begin{cases} \frac{1}{\eta_{charge}} \ for\ P_b(t) \le 0, & Charging \\ \frac{1}{\eta_{discharge}} \ for\ P_b(t) > 0, & Discharging \end{cases} \tag{23}$$

here, η_{charge} and $\eta_{discharge}$ describe the charging and discharging battery efficiencies, Δt describes the small increment in time, and Q_{bc} represents the capacity of the battery.

3.3. The model of the instantaneous power demand for the locomotive

This research considers HES based on battery and fuel cell to drive intercity passenger locomotives. Therefore, the mathematical modeling of the instantaneous power demand is significant. The locomotive model contains the force of friction between the railway track (F_{fr}) and the wheels, the aerodynamic drag (F_d), the force of acceleration (F_a), and force to overcome a slope (F_{sg}) as given below.

$$F_{\text{fr}} = M_{\text{et}} \times \frac{d\nu(t)}{dt} \tag{24}$$

$$F_{\text{sg}} = M_{\text{et}} \times g \times \sin\beta \tag{25}$$

$$F_d(t) = 0.5 \times D \times \rho \times \sigma \times \nu(t)^2 \tag{26}$$

$$F_{\text{fr}} = M_{\text{et}} \times g \times C_{Rr} \times \cos\beta \tag{27}$$

here, $\rho = 1.293\ \text{kg/m}^3$ describes the air density, σ is the cross-sectional area (m^2), D represents the drag coefficient, C_{Rr} describes the coefficient of rolling resistance, ν represents the locomotive velocity, and β is the gradient.

In the above equations, M_{et} describes the locomotive mass and is mathematically modeled as follows:

$$M_{\text{et}} = n_{ch} \times m_{ch} + M_{lcm} \tag{28}$$

here, n_{ch} describes the number of non-air-conditioned coaches, m_{ch} represents the mass of a non-air-conditioned coach, and M_{lcm} describes the mass of locomotive. Table 2 illustrates the parameters information for the studied HXD_3G locomotive that is taken from Li-xin (2010).

Table 2
The parameters information for the studied Chinese locomotive class HXD_3G.

Parameter	Value	Unit	Parameter	Value	Unit
Starting traction	584	kN	Axle load	25	t
Max. speed	120	Km/h	Power	9600	kW

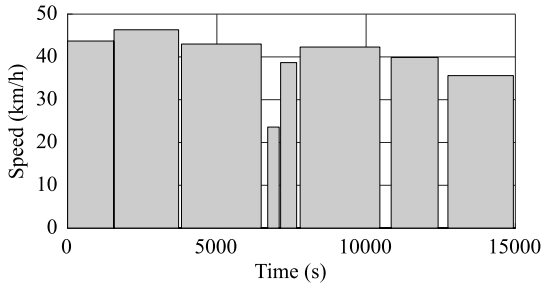

Fig. 5. Drive cycle for intercity passenger locomotive running in China.

Due to the fact that all the elements are non-air-conditioned coaches, this research considers only the mass of the non-air-conditioned coach. The instantaneous power demand for the locomotive is achieved as follows:

$$P_d = \left(\left(F_{\text{fr}}(t) + F_{\text{sg}}(t) + F_d(t) + F_{\text{fr}}(t)\right) \times \nu(t)\right)/\eta_s \tag{29}$$

here, η_s describes the transmission system performance that is considered 85%.

The total instantaneous power demand is as follows:

$$P_d^T(t) = P_{\text{aux}} + P_d(t) \tag{30}$$

here, P_{aux} summed up with the instantaneous power demand.

3.4. Drive cycles

The drive cycle is basically showing the speed variations of the locomotive during the time. The drive cycle is an important effective parameter on the instantaneous power demand of the locomotive. The studied drive cycle is based on the data from Jaafar et al. (2013). This data is provided using the mean value of the driving patterns followed by the locomotives. Fig. 5 shows the plot of the drive cycle and Table 3 illustrates the parameter values for the studied drive cycle.

4. Materials and methods

4.1. The method of energy management strategy

The main purpose of Energy Management Strategy (EMS) in the locomotive is to collect the instantaneous output power of the energy sources to provide the instantaneous power demand of the locomotive. Therefore, the EMS here is to make an instantaneous power trade-off between the locomotive power demand and HES output. The studied EMS includes the following considerations:

- The output power of the fuel cell is set to enhance at the acceleration time until it obtains the rated capacity of the fuel cell.
- The output power is then employed to operate at the obtained ratio until the locomotive decelerates.
- However, the rate of change of the fuel cell output power is limited by the rate constraint, the output power of the fuel cell has been decreased during braking and deceleration.
- The battery operates in both charging/discharging modes in the entire driving period based on the instantaneous power demand and the output power of the fuel cell.
- If the fuel cell output power is less than the instantaneous power demand, the battery has been discharged and if the fuel cell output power has a bigger value than the battery, the battery has been charged.

4.2. Design optimization model for the studied HES

The objective of this research is to optimal determining the battery and PEMFC sizes to develop the presented HES capability for supplying the time-dependent power demand of an intercity locomotive in China. The optimization purpose is to minimize the total cost of the components of the hybrid energy system. Since this optimization model should consider the cost of the battery, electric motor and also fuel cell, the cost function is considered as follows:

$$\min F(x) = f_b + f_m + f_{\text{FC}} + f_b^r + f_{\text{FC}}^r \tag{31}$$

here, f_b, f_m, and f_{FC} describe the cost of Li-Ion battery, the electric motor, and the fuel cell, respectively and f_{FC}^r and f_b^r describe the replacement costs of the battery and the fuel cell, respectively.

By considering the operational constraints such as output power variation of the PEM fuel cell and the battery SOC ($x = \left[P_{\text{FC}}^r, Q_{\text{FC}}^r\right]^T$):

$$SOC_{min} \le SOC(t) \le SOC_{max} \tag{32}$$

$$P_{dem}^T(t) = P_{\text{FC}}(t) + P_b(t) \tag{33}$$

$$P_{\text{FC}}^r \ge P_{dem}^{avg} \tag{34}$$

$$0 \le P_{\text{FC}}(t) \le P_{\text{FC}}^r \tag{35}$$

here, P_{FC}^r and Q_{FC}^r describe the fuel cell power rating and battery capacity, respectively, $C_{min} = 0.25$ and $C_{max} = 0.9$ describe the minimum and the maximum constraints of the SOC, respectively, $P_{dem}^T(t)$ describes the average power demand of the locomotive, $P_b(t)$ and $P_{\text{FC}}(t)$ describe the instantaneous power output of the battery and fuel cell, respectively, $P_{dem}^T(t)$ represents the total locomotive instantaneous power demand.

The reason for considering only the replacement cost of the fuel cell is that the only critical component of it is the part that contains the platinum catalyst, the polymer membrane, and the electrodes (Barbir and Gomez, 1997). The equations for the components have been given below:

$$f_b = f_{ub} \times Q_{\text{FC}}^r + C_b \tag{36}$$

$$f_m = f_{um} \times P_b^r + C_m \tag{37}$$

$$f_{\text{FC}} = f_{uFC} \times P_{\text{FC}}^r \tag{38}$$

$$f_b^r = \frac{V_b^{\text{fu}} \times M_r^b}{(1+R_i)^M} \tag{39}$$

$$f_{\text{FC}}^r = \frac{V_{\text{FC}}^{\text{fu}} \times N_r^{\text{FC}}}{(1+R_i)^N} \tag{40}$$

here, R_i describes the interest rate (here $R_i = 7\%$ (Wu et al., 2011)), $M(N)$ determine the life-time for the battery (PEM fuel cell) in years, $M_r^b(N_r^{\text{FC}})$ describe the number of replacements of the battery (PEM fuel cell), $f_{ub} = 652(\$/\text{kWh})$, $f_{um} = 22(\$/\text{kWh})$, and $f_{uFC} = 48(\$/\text{kWh})$, represent the cost of the battery, the electric motor, and the PEM fuel cell per unit rating respectively, $C_b = 679(\$)$ and $C_m = 420(\$)$ are the constant cost for the battery and the motor, respectively, V_b^{fu} and $V_{\text{FC}}^{\text{fu}}$ describe the future value of the battery and the PEM fuel cell, respectively (U. S. d. o. e. report).

Table 3
The parameters information for the studied Drive cycle.

Parameter	Value	Unit	Parameter	Value	Unit
Total driving time	15980	s	Average acceleration	0.5	m/s^2
Distance	220	km	Maximum deceleration	−0.7	m/s^2
Max. Speed	45	kmh	Average deceleration	−0.5	m/s^2
Average Speed	37.33	kmh	Max. acceleration	0.7	m/s^2

According to (U. S. d. o. e. report), the projected and the ultimately projected life-time of the PEM fuel cell for transportation in 2020 are 5000 and 8000 h. Therefore, by considering the operation of the passenger locomotive 9 h a day and the projected PEMFC life-time of 8000 operating hours, the value of N can be estimated as 3 years. In addition, based on U. S. d. o. e. report, the lifetime of a lithium-ion battery for replacement is ten years ($M = 10$). Therefore, by considering 20 years working period, the number for replacement of the PEM fuel cell and the battery are achieved one and three, respectively.

4.3. Basic Krill Herd algorithm

The Krill Herd (KH) algorithm was first introduced by Gandemi and Alavi to solve the optimization problems (Wang et al., 2014a,b; Wang and Yi, 2018; Wang et al., 2016a). The Krill Herd algorithm is categorized as one of the crowded intelligence algorithms, and it examines the mass movement of the krill to find food (Wang et al., 2014d, 2016b, 2019). Using this algorithm, we can solve NP-Hard class problems that do not have a precise solution in a reasonable time and find a sub-optimal solution for them. This algorithm is based on simulating the movements and behavior of a bunch of creatures to find food. In the Krill Herd algorithm, the minimum distance between each krill to food and the distance to the central population of the krill batch is assumed to be the cost function for the krill movement. The time-dependent location for each krill in the Krill Herd algorithm is formulated by three factors. The KH algorithm is inspired based on three main behaviors including explore to find food, random moving, and motivated motion based on the herd that can be modeled by a Lagrangian model for the ith krill as follows:

$$\frac{dX_i}{dt} = F_i + D_i + N_i \tag{41}$$

here, F_i describes the exploring to find food, D_i is the random moving behavior, and N_i represents the krill motivated motion based on the herd.

− Exploring to find food

This term contains two parts including food position and its previous experience. For the ith krill, it can be mathematically modeled as follows:

$$F_{i+1} = F_i \times \omega_f + V_f \times \beta_i \tag{42}$$

$$\beta_i = \beta_i^{\text{food}} + \beta_i^b \tag{43}$$

here, $\omega_f \in [0, 1]$ represents the inertia weight, V_f describes the speed of exploring, F_i describes the last exploring motion, β_i^{food} represents the food attractive and β_i^b represents the effect of the best cost of the ith krill so far.

− Random moving

Random moving is mainly a random process that is be formulated as follows:

$$D_i = D^{\max} \times \delta \tag{44}$$

here, D^{max} describes the maximum random speed, and δ describes the random vector in the range 0 and 1.

− Krill motivated motion based on the herd.

Based on the research, each of the krills attempts to keep itself close to the herd and move along with the mutual effects (Hofmann et al., 2004). The direction of motion α_i is divided into three parts including the local effect, the repulsive effect and the target effect. This can be mathematically modeled as follows:

$$N_{i+1} = N_i \times \omega_n + N_{\max} \times \alpha_i \tag{45}$$

here,

$$\alpha_i = \alpha_i^{le} + \alpha_i^T \tag{46}$$

here, N_i describes the last motivated motion, $\omega_n \in [0, 1]$ represents the inertia weight, N_{max} determines the maximum motivated speed, α_i^{le} describes the local effect, and α_i^T represents the target direction effect.

In the above equation, the local effect and the target direction effect are achieved by the following equations:

$$\alpha_i^{le} = \sum_{j=1}^{l} \hat{K}_{i,j} \times \hat{X}_{i,j} \tag{47}$$

$$\hat{K}_{i,j} = \frac{k_i - k_j}{k^w - k^b} \tag{48}$$

$$\hat{X}_{i,j} = \frac{X_j - X_i}{\left\|X_j - X_i\right\| + \epsilon} \tag{49}$$

$$\alpha_i^T = C^b \times \hat{K}_{i,b} \times \hat{X}_{i,b} \tag{50}$$

here, X determines the related positions, l describes the number of the neighbors, k_i and k_j describe the fitness of the ith and jth krill ($j = 1, 2, \ldots, l$), respectively, k^b and k^w are best and the worst fitness of the krill, respectively and C^b describes the effective coefficient of each krill with the best fitness to the ith krill individual.

The algorithm also uses genetic reproduction mechanisms including mutation and crossover operators. More details can be achieved by Gandomi and Alavi (2012).

4.4. Converged Krill Herd algorithm

In the present study, two main improvements have been employed for the KH algorithm. First, a self-adaptive weight is proposed to control the tendency of approaching the best optimal solution. For updating the location of the krills, random changes have been applied to the food exploring and the repulsive effect terms. Although using high exploring in the search space is so promising for initial iterations, at the final iterations, it is better to use exploitation and local search which helps to develop the algorithm population quality. This feature is applied to the food exploring and the repulsive effect terms as follows:

$$F_{i,\,new} = \begin{cases} F_i + \varphi_1 \times S\left(F_i\right) \otimes F_i, & \text{rand} > 0.5 \\ F_i - \varphi_1 \times S\left(F_i\right) \otimes F_i, & \text{rand} \le 0.5 \end{cases} \tag{51}$$

$$N_{i,\,new} = \begin{cases} N_i + \varphi_2 \times S\left(N_i\right) \otimes N_i, & \text{rand} > 0.5 \\ N_i - \varphi_2 \times S\left(N_i\right) \otimes N_i, & \text{rand} \le 0.5 \end{cases} \tag{52}$$

here,

$$\varphi_1 = \begin{cases} \left(\frac{f(F_{\text{best}})}{f(F_{\text{worst}})}\right)^2, & if\ f\left(F_{\text{worst}}\right) \neq 0 \\ 1 \quad , & if\ f\left(F_{\text{worst}}\right) = 0 \end{cases} \tag{53}$$

$$\varphi_2 = \begin{cases} \left(\frac{f(N_{\text{best}})}{f(N_{\text{worst}})}\right)^2, & if\ f\left(N_{\text{worst}}\right) \neq 0 \\ 1 \quad , & if\ f\left(N_{\text{worst}}\right) = 0 \end{cases} \tag{54}$$

Table 4
The general information about the benchmarks employed for the validation.

Type	Function	Equation	Optimal
Unimodal	Rotated high conditioned elliptic	$F_1(x) = f_1(M(x - o_1)) + F_1^*$	100
	Rotated bent cigar	$F_2(x) = f_2(M(x - o_2)) + F_2^*$	200
	Rotated discuss	$F_3(x) = f_3(M(x - o_3)) + F_3^*$	300
Multimodal	Shifted and rotated Rosenbrock	$F_4(x) = f_4\left(M\left(\frac{2.048(x-o_4)}{100}\right)\right) + F_4^*$	400
	Shifted and rotated Ackley	$F_5(x) = f_5(M(x - o_1)) + F_8^*$	500

Table 5
The benchmark functions utilized in the validation.

Type	ID	Function	f^*
Unimodal	f_1	Rotated high conditioned elliptic function	100
	f_2	Rotated bent cigar function	200
	f_3	The function of Rotated discus function	300
Multimodal	f_4	Shifted and rotated Rosenbrock function	400
	f_5	Shifted and rotated Ackley's function	500

here, $f(F_{\text{worst}})$, N_{worst}, and $f(F_{\text{best}})$, N_{best} describe the cost function values of the worst solution and best solution, respectively.

In this technique, the value of the presented weight is increased gradually to reduce the difference between the worst and the best solutions. This technique also does not require any Another advantage of this technique is that there is no need for parameter adjusting.

This study also uses a chaotic mechanism for improving system exploration. The best solution for each iteration is significant such that the other entire krill herd attempt to move based on the best solution experience to get better results. However, sometimes the best solution may be stuck in the local optimum. This problem makes a misleading solution to the other krill individuals to follow the best individual that finally leads to premature convergence.

To resolve this problem, the random moving equation has been reformulated based on chaos theory. Chaotic mechanisms have ergodic and sequence random characteristics that are very helpful to improve the algorithm premature convergence (Yang et al., 2007; Rim et al., 2018). Here, the well known logistic map mechanism has been used for this purpose. Applying this improvement on the random moving gives the following formulation:

$$D_{i+1}^{\text{new}} = D_i^{\text{new}} + \sigma_i \times D_i^{\text{new}} \tag{55}$$

where,

$$\sigma_{i+1} = 4\sigma_i(1 - \sigma_i) \tag{56}$$

here, σ_i determines the value for the ith chaotic iteration, and the initial value $\sigma_1 \in [0, 1]$ describes a random value.

4.5. Algorithm validation

For validating the performance of the presented algorithm, five benchmarks are employed and the results are compared with some different bio-inspired algorithms such as gravitational search algorithm (GSA) (Rashedi et al., 2009), emperor penguin optimization (EPO) (Dhiman and Kumar, 2018), world cup optimization algorithm (WCO) (Razmjooy et al., 2016), and the original KH (Gandomi and Alavi, 2012) to show the system efficiency. Table 4 illustrates the information about the utilized benchmarks for the algorithm validation

Table 5 illustrates the benchmark functions utilized in the validation.

The population size for all algorithms is considered 100, function evaluations are 100,000 for all functions, and the stopping criteria is based on a maximum number of function calculation (Khalilpuor et al., 2001; Namadchian et al., 2016; Razmjooy and Ramezani, 2016). The dimension is 30 ($n = 30$). The best efficiency is achieved by over 55 runs in Table 6 for all functions. Here, "std" describes the standard deviation, "Median" represents the median of the result fitness values, and "maximum" and "minimum" are the maximum and minimum fitness values for each algorithm, respectively.

Table 6 illustrates that the presented algorithm has the best results than the other compared algorithms for the analyzed benchmarks.

In order to judge whether the results of a proposed method are significant, a nonparametric statistical test called Wilcoxon's rank-sum test has been carried out. Wilcoxon signed ranks test investigate if there are two samples from two unlike populations. In the Wilcoxon test, the dominance of the two algorithms is determined based on the hypothesis test that is described by the null hypothesis (H0) and the alternative hypothesis (H1). If there is an alteration between two algorithms, the hypothesis is alternative and if there is no alteration between two algorithms, the hypothesis is null. More explanation can be found in Wang et al. (2014c).

In this study, the Wilcoxon signed-rank test is adopted for statistical validation of the superiority of the MEHO algorithm toward the analyzed algorithms. Table 7 indicates the p-values obtained by Wilcoxon signed-rank test.

CKH vs	GSA (Rashedi et al., 2009)	EPO Dhiman and Kumar (2018)	WCO (Razmjooy et al., 2016)	KH (Gandomi and Alavi, 2012)
	5.12e−4	8.27e−4	4.87e−4	0.0115

As can be seen, the P-values are very small that illustrate the important outperformance of CKH over all other compared algorithms except the KH algorithm. However, in this dimension, CKH outperforms KH, its p-value is not small enough.

4.6. System solution based on CKH algorithm

In this research, the proposed CKH algorithm is employed for determining the optimal sizes for the PEM fuel cell and the battery to provide the minimum total cost of the hybrid energy system. Here, the sizes information for both battery and PEM fuel cell have been encoded by the Krill in CKH algorithm. The CKH algorithm is then embedded by the proposed EMS (Section 3) as the support subroutine. Fig. 6 shows the general diagram of the proposed methodology.

5. Simulation results

This section analyzes the results of the introduced hybrid energy system (HES) system. As aforementioned, the primary objective of this study is to achieve the minimum value for the total cost of the HES by determining the sizes of the battery and the PEM fuel cell based on an optimal solution. A definite drive

Table 6
Comparative results of the algorithms.

		GSA (Rashedi et al., 2009)	EPO (Dhiman and Kumar, 2018)	WCO (Razmjooy et al., 2016)	KH (Gandomi and Alavi, 2012)	CKH
f_1	Maximum	5.27E+07	7.98E+07	3.24E+06	1.05E+06	2.83E+05
	Minimum	4.73E+06	6.14E+06	3.27E+05	1.16E+05	2.45E+04
	Median	7.96E+06	1.97E+07	1.28E+06	5.32E+05	1.58E+05
	std	2.26E+07	2.53E+07	6.13E+05	3.47E+05	1.01E+05
f_2	Maximum	2.71E+04	7.86E+06	3.69E+04	2.39E+03	1.35E+03
	Minimum	2.98E+03	1.45E+06	5.78E+03	2.64E+02	1.95E+02
	Median	7.84E+03	4.06E+06	1.76E+04	4.52E+02	3.16E+02
	std	3.15E+03	1.73E+06	9.20E+03	2.41E+02	2.01E+02
f_3	Maximum	7.62E+04	4.96E+04	1.67E+04	1.93E+03	1.23E+03
	Minimum	1.98E+04	6.37E+02	3.62E+03	4.81E+02	3.36E+02
	Median	5.23E+04	8.24E+03	7.82E+03	2.11E+02	4.27E+02
	std	9.14E+03	1.69E+04	3.48E+03	3.48E+02	2.30E+02
f_4	Maximum	7.91E+02	5.87E+02	5.16E+02	2.20E+02	5.16E+02
	Minimum	6.17E+02	3.80E+02	3.52E+02	3.86E+02	2.85E+02
	Median	7.42E+02	6.19E+02	4.97E+02	4.53E+02	4.01E+02
	std	4.81E+01	4.01E+01	3.14 E+01	3.54E+01	3.48E+01
f_5	Maximum	5.20E+02	5.20E+02	5.20E+02	5.14E+02	20E+02
	Minimum	5.20E+02	5.20E+02	5.20E+02	5.20E+02	5.20E+02
	Median	5.20E+02	5.20E+02	5.20E+02	5.20E+02	5.20E+02
	std	4.78E−03	3.85E−04	4.19E−03	4.8E−04	6.98E−05

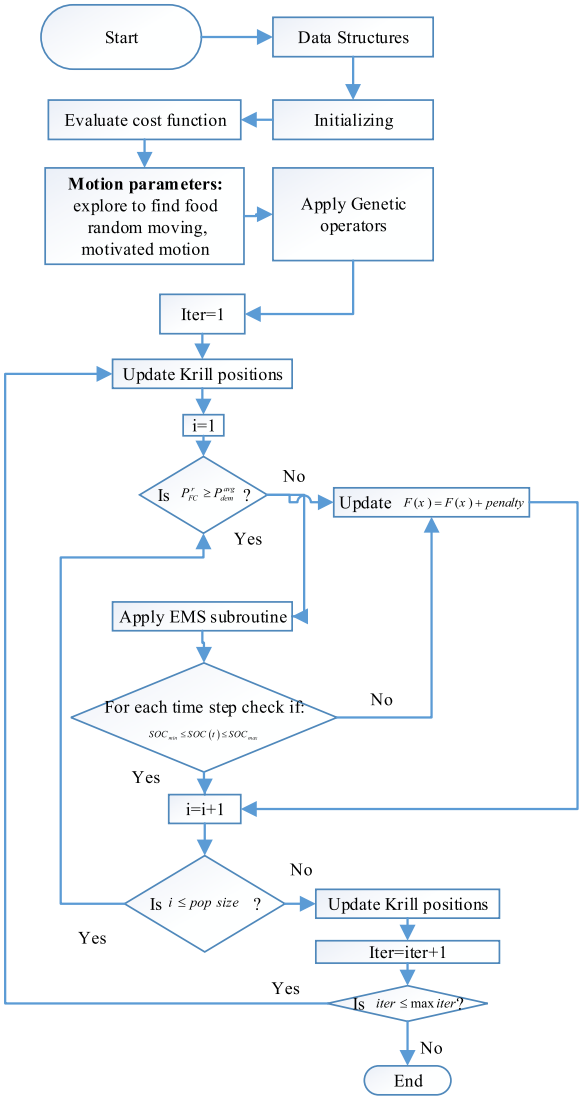

Fig. 6. The flowchart diagram of the proposed solution strategy.

Table 7
The selected parameters for the CKH algorithm.

Parameter	Value
No. of Krill herd population	50
No. of iteration	500
explore to find food	0.05
motivated motion	0.005

cycle has been utilized here (Section 4.2) such that the average power demand (P^{avg}_{dem}) of it corresponding to 0%, 1%, and 2% slope of the railway track (β) are considered 3.1 MW, 3.7 MW, and 3.9 MW, respectively. At the beginning of the drive cycle, the initial value for SOC, ($SOC_{initial}$) is assumed to be 0.7. Table 7 illustrates the selected parameters for the CKH algorithm after multiple trials and errors.

Table 8 shows the optimum sizes of the PEM fuel cell and the battery for the considered drive cycle based on the proposed CKH algorithm and its comparison with the PSO algorithm and the typical KH algorithm. Here, three different values for the slope have been considered. Table 8 illustrates that by increasing the percentage of slope, the required power demand for both battery and fuel cell has been increased.

Furthermore, it is clear that using the presented CKH algorithm gives a larger size for the PEM fuel cell in energy management. Totally, the difference among the three algorithms (EMS) is that the required battery size for the system in PSO is larger than the KH algorithm and in the KH algorithm is larger than the CKH and due to the high cost of battery technology, the proposed CKH algorithm is better selection for this purpose, i.e. whatever the size of the fuel cell has been increased, we need a battery with smaller size.

In the following, the dynamic behavior of the HES has been analyzed. Fig. 7 show the diagram of the output power of the battery and the fuel cell variations and SOC variation with time. The figure declares that the battery should be discharged when the locomotive power demand exceeds the output power of the PEM fuel cell. This happens when the locomotive has a speed higher than the average speed of the drive cycles that reduce the battery SOC at this time. In contrast, the battery has been charged when the locomotive has a lower speed than the average speed which increases the battery SOC.

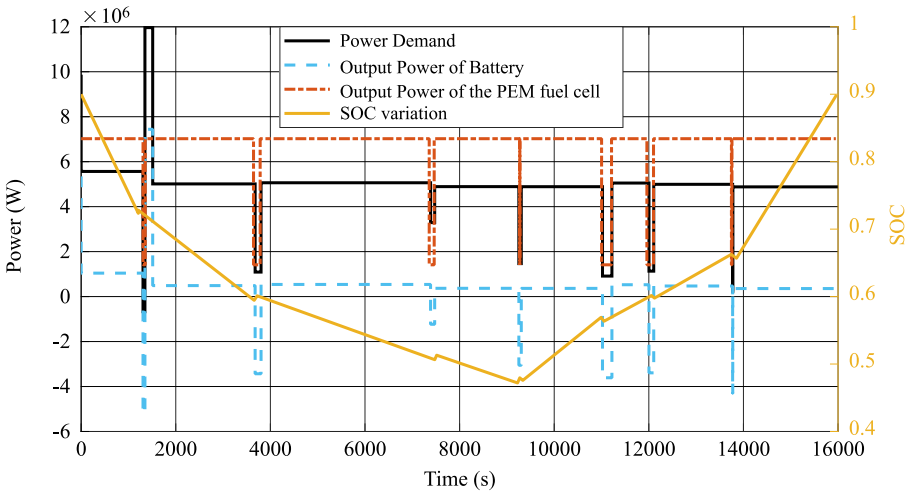

Fig. 7. The variation of battery output power and PEM fuel cell output power and variation of SOC with time for EMS without slope.

Table 8
The optimum sizes of the PEM fuel cell and the battery for the considered drive cycle based on different algorithms.

	CKH		KH		PSO	
Slope (%)	P^r_{FC} (MWh)	Q^r_b (MWh)	P^r_{FC} (MWh)	Q^r_b (MWh)	P^r_{FC}(MWh)	Q^r_b (MWh)
0	4.52	3.19	4.12	3.51	3.59	4.61
1	5.13	3.85	4.93	4.22	4.30	5.17
2	5.84	4.43	5.57	4.48	5.03	5.84

Table 9
The results of the total cost for HES in ($) based on different algorithms.

Slope (%)	CKH	KH	PSO
0	3.15×10^6	3.47×10^6	3.74×10^6
1	3.56×10^6	4.01×10^6	4.27×10^6
2	3.93×10^6	4.56×10^6	4.72×10^6

Table 9 illustrates the results of the total cost for HES in ($). Simulation results declare that the HES total cost in PSO is the highest and this cost is the lowest based on the proposed CKH strategy for energy management that is because larger battery size needs higher cost.

6. Conclusions

This study presented an optimized methodology for optimal size selection of a battery and a PEM fuel cell to provide a hybrid energy system to supply the power demand of an intercity locomotive. The main purpose was to minimize the total cost of the hybrid energy system including the replacement cost of the fuel cell stack and the battery during the planning period. The energy management strategy here considers both battery and fuel cell with instantaneous variations in their power output. To achieve the best sizes of the fuel cell and the battery for the minimum cost, a new improved version of the Krill Herd (KH) algorithm was introduced. The results were analyzed based on the average power demand, speed demand of the locomotive, and the locomotive slope. The results of the presented CKH algorithm were compared with the standard KH and PSO algorithm and the results showed that the total cost of the CKH needs the minimum value. The improvements in this paper can be also applied to other new optimization algorithms like monarch butterfly optimization (MBO), earthworm optimization algorithm (EWA), elephant herding optimization (EHO), moth search (MS) algorithm.

Declaration of competing interest

The authors declare that they have no known competing financial interests or personal relationships that could have appeared to influence the work reported in this paper.

CRediT authorship contribution statement

Yingying Guo: Conceptualization, Data curation, Writing - original draft, Writing - review & editing. **Xiangdong Dai:** Conceptualization, Data curation, Writing - original draft, Writing - review & editing. **Kittisak Jermsittiparsert:** Conceptualization, Data curation, Writing - original draft, Writing - review & editing. **Navid Razmjooy:** Conceptualization, Data curation, Writing - original draft, Writing - review & editing.

Acknowledgment

Cultural and art science research project of the Ministry of culture: Research on the modern disconnection and the contemporary innovation of Chinese traditional furniture art (No. 15DG53).

Finally, thanks Emate for language service.

References

Aghajani, Gholamreza, Ghadimi, Noradin, 2018. Multi-objective energy management in a micro-grid. Energy Rep. 4, 218–225.

Akbary, Paria, et al., 2019. Extracting appropriate nodal marginal prices for all types of committed reserve. Comput. Econ. 53 (1), 1–26.

Aouali, F.Z., Becherif, M., Ramadan, H.S., Emziane, M., Khellaf, A., Mohammedi, K., 2017. Analytical modelling and experimental validation of proton exchange membrane electrolyser for hydrogen production. Int. J. Hydrogen Energy 42 (2), 1366–1374.

Bagal, H.A., Soltanabad, Y.N., Dadjuo, M., Wakil, K., Ghadimi, N., 2018. Risk-assessment of photovoltaic-wind-battery-grid based large industrial consumer using information gap decision theory. Sol. Energy 169, 343–352.

Barbir, F., Gomez, T., 1997. Efficiency and economics of proton exchange membrane (PEM) fuel cells. Int. J. Hydrogen Energy 22 (10–11), 1027–1037.

Bendjedia, B., Rizoug, N., Boukhnifer, M., Bouchafaa, F., Benbouzid, M., 2018. Influence of secondary source technologies and energy management strategies on energy storage system sizing for fuel cell electric vehicles. Int. J. Hydrogen Energy 43 (25), 11614–11628.

Corrêa, J.M., Farret, F.A., Canha, L.N., Simoes, M.G., 2004. An electrochemical-based fuel-cell model suitable for electrical engineering automation approach. IEEE Trans. Ind. Electron. 51 (5), 1103–1112.

Dhiman, G., Kumar, V., 2018. Emperor penguin optimizer: a bio-inspired algorithm for engineering problems. Knowl.-Based Syst. 159, 20–50.

Dongmin, Yu., et al., 2019. Dynamic multi agent-based management and load frequency control of PV/Fuel cell/wind turbine/CHP in autonomous microgrid system. Energy 173, 554–568.

Dongmin, Yu., et al., 2020. Energy management of wind-PV-storage-grid based large electricity consumer using robust optimization technique. J. Energy Storage 27, 101054.

Eslami, Mahdiyeh, et al., 2019. A new formulation to reduce the number of variables and constraints to expedite SCUC in bulky power systems. Proc. Natl. Acad. Sci. India A 89 (2), 311–321.

Firouz, M.H., Ghadimi, N., 2015. Wind energy uncertainties in multi-objective environmental/economic dispatch based on multi-objective evolutionary algorithm. UCT J. Res. Sci. Eng. Technol. 3 (3), 8–15.

Firouz, Hosseini, Mansour, Ghadimi, Noradin, 2016. Optimal preventive maintenance policy for electric power distribution systems based on the fuzzy AHP methods. Complexity 21 (6), 70–88.

Gandomi, A.H., Alavi, A.H., 2012. Krill herd: a new bio-inspired optimization algorithm. Commun. Nonlinear Sci. Numer. Simul. 17 (12), 4831–4845.

Gao, W., Darvishan, A., Toghani, M., Mohammadi, M., Abedinia, O., Ghadimi, N., 2019. Different states of multi-block based forecast engine for price and load prediction. Int. J. Electr. Power Energy Syst. 104, 423–435.

Geng, B., Mills, J., Sun, D., 2014. Combined power management/design optimization for a fuel cell/battery plug-in hybrid electric vehicle using multi-objective particle swarm optimization. Int. J. Automot. Technol. 15 (4), 645–654.

Ghadimi, N., 2015. An adaptive neuro-fuzzy inference system for islanding detection in wind turbine as distributed generation. Complexity 21 (1), 10–20.

Gollou, Abbas Rahimi, Ghadimi, Noradin, 2017. A new feature selection and hybrid forecast engine for day-ahead price forecasting of electricity markets. J. Intell. Fuzzy Systems 32 (6), 4031–4045.

Haixiong, Ye, et al., 2020. High step-up interleaved dc/dc converter with high efficiency. Energy Sources A 1–20.

Hamian, Melika, et al., 2018. A framework to expedite joint energy-reserve payment cost minimization using a custom-designed method based on mixed integer genetic algorithm. Eng. Appl. Artif. Intell. 72, 203–212.

Hofmann, E.E., Haskell, A.E., Klinck, J.M., Lascara, C.M., 2004. Lagrangian modelling studies of Antarctic krill (Euphausia superba) swarm formation. ICES J. Mar. Sci. 61 (4), 617–631.

Homayoun, Ebrahimian, et al., 2018. The price prediction for the energy market based on a new method. Econ. Res.-Ekonomska istraživanja 31 (1), 313–337.

Hong, Z., Li, Q., Han, Y., Shang, W., Zhu, Y., Chen, W., 2018. An energy management strategy based on dynamic power factor for fuel cell/battery hybrid locomotive. Int. J. Hydrogen Energy 43 (6), 3261–3272.

Hosseini, H., Farsadi, M., Khalilpour, M., Razmjooy, N., 2011. Hybrid energy production system with PV array and wind turbine and pitch angle optimal control by genetic algorithm (GA).

Hosseini, H., Farsadi, M., Lak, A., Ghahramani, H., Razmjooy, N., 2012. A novel method using imperialist competitive algorithm (ICA) for controlling pitch angle in hybrid wind and PV array energy production system. Int. J. Tech. Phys. Probl. Eng. (11), 145–152.

Hosseini, H., Tousi, B., Razmjooy, N., Khalilpour, M., 2013. Design robust controller for automatic generation control in restructured power system by imperialist competitive algorithm. IETE J. Res. 59 (6), 745–752.

Jaafar, A., Sareni, B., Roboam, X., 2013. A systemic approach integrating driving cycles for the design of hybrid locomotives. IEEE Trans. Veh. Technol. 62 (8), 3541–3550.

Kandidayeni, M., Macias, A., Khalatbarisoltani, A., Boulon, L., Kelouwani, S., 2019. Benchmark of proton exchange membrane fuel cell parameters extraction with metaheuristic optimization algorithms. Energy.

Khalilpuor, M., Razmjooy, N., Hosseini, H., Moallem, P., 2011. Optimal control of DC motor using invasive weed optimization (IWO) algorithm, in: Majlesi Conference on Electrical Engineering, Majlesi Town, Isfahan, Iran.

Khodaei, Hossein., et al., 2018. Fuzzy-based heat and power hub models for cost-emission operation of an industrial consumer using compromise programming. Appl. Therm. Eng. 137, 395–405.

Leng, Hua, et al., 2018. A new wind power prediction method based on ridgelet transforms, hybrid feature selection and closed-loop forecasting. Adv. Eng. Inform. 36, 20–30.

Li-xin, Q., 2010. The world latest progress of heavy railway transportation technology. Electr. Drive Locomotives 1, 3–7.

Liu, Yang, Wang, Wei, Ghadimi, Noradin, 2017. Electricity load forecasting by an improved forecast engine for building level consumers. Energy 139, 18–30.

Luo, X., Wang, J., Dooner, M., Clarke, J., 2015. Overview of current development in electrical energy storage technologies and the application potential in power system operation. Appl. Energy 137, 511–536.

Maleki, A., Rosen, M.A., 2017. Design of a cost-effective on-grid hybrid wind–hydrogen based CHP system using a modified heuristic approach. Int. J. Hydrogen Energy 42 (25), 15973–15989.

Mirzapour, Farzaneh, et al., 2019. A new prediction model of battery and wind-solar output in hybrid power system. J. Ambient Intell. Humaniz. Comput. 10 (1), 77–87.

Namadchian, A., Ramezani, M., Razmjooy, N., 2016. A new meta-heuristic algorithm for optimization based on variance reduction of guassian distribution. Majlesi J. Electr. Eng. 10 (4), 49.

Rashedi, E., Nezamabadi-Pour, H., Saryazdi, S., 2009. GSA: a gravitational search algorithm. Inform. Sci. 179 (13), 2232–2248.

Razmjooy, N., Khalilpour, M., Ramezani, M., 2016. A new meta-heuristic optimization algorithm inspired by FIFA world cup competitions: theory and its application in PID designing for AVR system. J. Control Autom. Elect. Syst. 27 (4), 419–440.

Razmjooy, M., Ramezani, M., 2016. Model Order Reduction based on meta-heuristic optimization methods, in: 1st International Conference on New Research Achievements in Electrical and Computer Engineering Iran.

Razmjooy, N., Ramezani, M., Estrela, V.V., Loschi, H.J., do Nascimento, D.A., 2018. Stability analysis of the interval systems based on linear matrix inequalities. In: Brazilian Technology Symposium. Springer, pp. 371–378.

Rim, C., Piao, S., Li, G., Pak, U., 2018. A niching chaos optimization algorithm for multimodal optimization. Soft Comput. 22 (2), 621–633.

Saeedi, Mohammadhossein., et al., 2019. Robust optimization based optimal chiller loading under cooling demand uncertainty. Appl. Therm. Eng. 148, 1081–1091.

Seyed-Shenava, S.-J., Khezri, O., 2014. Optimal PID controller designing for voltage control of fuel cell. Bull. Electr. Eng. Inform. 3 (4), 229–238.

Shamel, A., Ghadimi, N., 2016. Hybrid PSOTVAC/BFA technique for tuning of robust PID controller of fuel cell voltage.

U. S. d. o. e. report, Section 3.4 Fuel Cells – Department of Energy. United State department of energy report https://www.energy.gov/sites/prod/files/2016/06/f32/fcto_myrdd_fuel_cells_0.pdf (accessed).

Wang, G.-G., Deb, S., Gandomi, A.H., Alavi, A.H., 2016a. Opposition-based krill herd algorithm with cauchy mutation and position clamping. Neurocomputing 177, 147–157.

Wang, G.-G., Gandomi, A.H., Alavi, A.H., 2014a. An effective krill herd algorithm with migration operator in biogeography-based optimization. Appl. Math. Model. 38 (9–10), 2454–2462.

Wang, G.-G., Gandomi, A.H., Alavi, A.H., 2014b. Stud krill herd algorithm. Neurocomputing 128, 363–370.

Wang, G.-G., Gandomi, A.H., Alavi, A.H., Gong, D., 2019. A comprehensive review of krill herd algorithm: variants, hybrids and applications. Artif. Intell. Rev. 51 (1), 119–148.

Wang, G.-G., Gandomi, A.H., Yang, X.-S., Alavi, A.H., 2016b. A new hybrid method based on krill herd and cuckoo search for global optimisation tasks. Int. J. Bio-Inspired Comput. 8 (5), 286–299.

Wang, G.-G., Guo, L., Gandomi, A.H., Hao, G.-S., Wang, H., 2014c. Chaotic krill herd algorithm. Inform. Sci. 274, 17–34.

Wang, G., Guo, L., Wang, H., Duan, H., Liu, L., Li, J., 2014d. Incorporating mutation scheme into krill herd algorithm for global numerical optimization. Neural Comput. Appl. 24 (3–4), 853–871.

Wang, H., Yi, J.-H., 2018. An improved optimization method based on krill herd and artificial bee colony with information exchange. Memetic Comput. 10 (2), 177–198.

Wu, X., Cao, B., Li, X., Xu, J., Ren, X., 2011. Component sizing optimization of plug-in hybrid electric vehicles. Appl. Energy 88 (3), 799–804.

Yang, D., Li, G., Cheng, G., 2007. On the efficiency of chaos optimization algorithms for global optimization. Chaos Solitons Fractals 34 (4), 1366–1375.